On the geometry of fracture and frustration

Koning, V.

1

INTRODUCTION

1.1 GEOMETRIC FRUSTRATION

Whether it concerns biological matter such as membranes, DNA and viruses, or synthesised anisotropic colloidal particles, the deformations inherent to soft matter almost inevitably call for a geometric description. Therefore, the use of geometry has always been essential in our understanding of the physics of soft matter. However, only recently has geometry turned into an instrument for the design and engineering of novel materials. Key concepts are geometrical frustration and the topological defects that are often a consequence of this frustration [81, 72, 37, 6].

Geometrical frustration refers to the impossibility of local order to propagate throughout a chosen space. This impossibility is of geometric nature and could for instance be due to the topology of the space. Probably your first and most familiar encounter with this phenomenon was while playing (association) football. The mathematically inclined amongst you may have wandered off during the game and wondered: "Why does the ball contain hexagonal *and* pentagonal panels?" The ball cannot contain hexagonal panels only: a perfect tiling of hexagons (an example of local order) cannot be achieved on the spherical surface (the space considered). There exists a constraint on the number of faces, F, edges, E, and vertices, V. The constraint is named after Euler and reads [65]

$$F - E + V = \chi, \tag{1}$$

where χ is the Euler characteristic. The Euler characteristic is a quantity insensitive to continuous deformations of the surface of the ball such as twisting and bending. We call such quantities topological. Only if one would perform violent operations such as cutting a hole in the sphere and glueing a handle to the hole would a surface of differently topology be created [65, 69]. For a surface with one handle $\chi = 0$, just as for a torus or a coffee mug. The Euler characteristic χ equals 2 for the spherical surface of the ball. Thus, Euler's polyhedral formula (eq. (1)) ensures

the need of 12 pentagonal patches besides the hexagonal ones, no matter how well inflated the ball is. To see this, write the number of faces F as the sum of the number of hexagons, H, and pentagons, P, i.e. $F = H + P$. One edge is shared by two faces, hence $E = \frac{1}{2}(6H + 5P)$. Moreover, each vertex is shared among three faces, hence $V = \frac{1}{3}(6H + 5P)$. Substituting the expressions for F, E and V into eq. (1) yields $P = 12$. These pentagons are the defects. Similarly, protein shells of spherical viruses which enclose the genetic material consist of pentavalent and hexavalent subunits [9, 52]. Another condensed matter analog of the geometrically frustrated football is the 'colloidosome'. Colloidosomes are spherical colloidal crystals [21, 4, 34] that are of considerable interest as microcapsules for delivery and controlled release of drugs [21].

Figure 1: *Left panel:* Geometric frustration in a football. A perfect tiling of hexagonal panels cannot be achieved everywhere, resulting in black pentagonal panels (defects). *Right panel:* Geometric frustration on the globe. The lines of latitude shrink to a point at the north and south poles (defects). Adapted from ref. [1].

Another common example of geometric frustration are the lines of latitude on the surface of a globe. The points where these lines shrink to a point, that is, the North and South Poles, are the defects. Just like the pentagons on the football, the defects on the globe are also required by a topological constraint, namely the Poincare-Hopf theorem [69]:

$$\sum_a s_a = \chi. \tag{2}$$

The lines of latitude circle once around both poles. Hence, there are two defects with a unit winding number, s. (See section 1.5 for a more precise definition.) Similar to the lines of longitude and latitude on the globe, a coating of a nanoparticle with a monolayer of ordered tilted molecules also has two polar defects [58, 57, 70, 105, 20]. Recently, Stellacci and co-workers have been able to functionalise the defects to assemble linear chains of nanoparticles [20]. A nematic liquid crystal coating possesses four defects at the vertices of a regular tetrahedron in the ground state [57]. Attaching chemical linkers to these defects could result in a three-dimensional diamond structure [70], rather than a one-dimensional chain. Functionalisation of the defects, thus resulting from ordered structures confined to curved spaces, offers an intriguing route to directed assembly.

The types of order that we will discuss in this introductory chapter are crystalline and nematic liquid crystalline (1.2). After introducing mathematical preliminaries in section 1.3, we will discuss the elasticity of crystals and liquid crystals (section 1.4) and give a classification of the defects in these phases of matter (section 1.5). We will elucidate the role of geometry in this subject. In particular, we will explicitly show that, in contrast to the two examples given in the introduction, a topological constraint is not necessary for geometric frustration. In section 1.6 we will review coupling between defects and curvature. Nematic order on the sphere is discussed in section 1.7.

This thesis is outlined thoroughly in section 1.8. Subsections 1.8.1 and 1.8.2 (corresponding to Part I and II, respectively) are about nematic liquid crystals confined to various geometries. In some aspects a nematic liquid crystal behaves like a liquid. Indeed, one can capture a nematic in the form of droplets or in containers of various shapes, just as one can do that for liquid water. At the same time nematic liquid crystals exhibit, just as crystals, anisotropy: in a nematic the molecules self-organise. Our goal in Part I and II is to explore avenues to control this molecular assembly geometrically by tuning the shape of the boundary of the nematic liquid crystal. Our interest in part III (subsection 1.8.3) is the integrity and failure of curved materials. It may, for instance, be very relevant to know under which conditions a colloidosome fractures. Part III discusses crack growth in curved elastic films.

1.2 LIQUID CRYSTALS

Besides the familiar solid, liquid and gas phases, there exist other fascinating forms of matter, which display phenomena with order intermediate between conventional isotropic fluids and crystalline solids. These are therefore called liquid crystalline or mesomorphic phases [18, 95]. Let us consider the difference between a solid crystal and a liquid crystal. In a solid crystal all the constituents are located in a periodic fashion, such that only specific translations return the same lattice. Moreover, the bonds connecting neighbouring crystal sites define a discrete set of vectors which are the same throughout the system. In a crystal, there is thus both bond-orientational and translational order. In liquid crystals there is orientational order, as the anisotropic constituent molecules define a direction in space, but the translational order is partially or fully lost. The latter phase, in which there is no translational order whatsoever, is called a nematic liquid crystal. The mobility of the translationally disordered molecules is responsible for the fluidic properties of nematic liquid crystals.

1.3 DIFFERENTIAL GEOMETRY OF SURFACES

1.3.1 *Preliminaries*

For a thorough introduction to the differential geometry of surfaces, please consult refs. [97, 17, 37]. In this section we will introduce the topic briefly and establish the notation. Points on a curved surface embedded in the three dimensional world we live in can be described by a three-component vector $\mathbf{R}(\mathbf{x})$ as a function of the coordinates $\mathbf{x} = \left(x^1, x^2\right)$. Vectors tangent to this surface are given by

$$\mathbf{t}_\alpha = \partial_\alpha \mathbf{R}, \tag{3}$$

where $\partial_\alpha = \frac{\partial}{\partial x^\alpha}$ is the partial derivative with respect to x^α. These are in in general neither normalised nor orthogonal. However, it does provide a basis in which to express an arbitrary tangent vector $\mathbf{n}$ in:

$$\mathbf{n} = n^\alpha \mathbf{t}_\alpha. \tag{4}$$

Here we have used the Einstein summation convention, *i.e.*, an index occurring twice in a single term is summed over, provided that one of the them is a lower (covariant) index and the other is an upper (contravariant) index. We reserve Greek characters α, β, $\gamma, \ldots$ as indices for components of vectors and tensors tangent to the surface. The so-called metric tensor reads

$$g_{\alpha\beta} = \mathbf{t}_\alpha \cdot \mathbf{t}_\beta, \tag{5}$$

and its inverse is defined by

$$g^{\alpha\beta} g_{\beta\gamma} = \delta^\alpha_\gamma, \tag{6}$$

where δ^α_γ is equal to one if $\alpha = \gamma$ and zero otherwise. We can lower and raise indices with the metric tensor and inverse metric tensor, respectively, in the usual way, *e.g.*

$$g_{\alpha\beta} n^\alpha = n_\beta \tag{7}$$

It is straightforward to see that the inner product between two vectors $\mathbf{n}$ and $\mathbf{m}$ is

$$\mathbf{n} \cdot \mathbf{m} = n^\alpha \mathbf{t}_\alpha \cdot m^\beta \mathbf{t}_\beta = g_{\alpha\beta} n^\alpha m^\beta = n^\alpha m_\alpha. \tag{8}$$

The area of the parallelogram generated by the infinitesimal vectors $dx^1\mathbf{t}_1$ and $dx^2\mathbf{t}_2$, is given by the magnitude of their cross product, and yields the area element

$$\begin{aligned} dS &= \left| dx^1 \mathbf{t}_1 \times dx^2 \mathbf{t}_2 \right| \\ &= \sqrt{(\mathbf{t}_1 \times \mathbf{t}_2)^2} dx^1 dx^2 \\ &= \sqrt{|\mathbf{t}_1|^2 |\mathbf{t}_2|^2 - (\mathbf{t}_1 \cdot \mathbf{t}_2)^2} dx^1 dx^2 \\ &= \sqrt{g_{11} g_{22} - g_{12} g_{21}} dx^1 dx^2 \\ &= \sqrt{g} d^2x, \end{aligned} \tag{9}$$

where $g = \det(g_{\alpha\beta})$, the determinant of the metric tensor, and d^2x is shorthand for $dx^1 dx^2$. More generally, the magnitude of the cross product of two vectors $\mathbf{m}$ and $\mathbf{n}$ is

$$|\mathbf{m} \times \mathbf{n}| = \left| \gamma_{\alpha\beta} m^\alpha n^\beta \right|, \tag{10}$$

which introduces the antisymmetric tensor

$$\gamma_{\alpha\beta} = \sqrt{g} \epsilon_{\alpha\beta}, \tag{11}$$

where $\epsilon_{\alpha\beta}$ is the Levi-Civita symbol satisfying $\epsilon_{12} = -\epsilon_{21} = 1$ and is zero otherwise.

Since we will encounter tangent unit vectors, *e.g.* indicating the orientation of some physical quantity, it is convenient to decompose this vector in a set of orthonormal tangent vectors, $\mathbf{e}_1(\mathbf{x})$ and $\mathbf{e}_2(\mathbf{x})$, such that

$$\mathbf{e}_i \cdot \mathbf{e}_j = \delta_{ij} \quad \text{and} \quad \mathbf{N} \cdot \mathbf{e}_i = 0, \tag{12}$$

alternative to the basis defined in eq. 3. Here $\mathbf{N}$ is the vector normal to the surface. We use the Latin letters i, j and k for the components of vectors expressed in this orthonormal basis. As they are locally Cartesian, they do not require any administration of the position of the index. Besides the area element, we need a generalisation of the partial derivative. This generalisation is the covariant derivative, D_α, the projection of the derivative onto the surface. The covariant derivative of $\mathbf{n}$ expressed in the orthonormal basis reads in component form [37]

$$\begin{aligned} D_\alpha n_i &= \mathbf{e}_i \cdot \partial_\alpha \mathbf{n} \\ &= \mathbf{e}_i \cdot \partial_\alpha n_j \mathbf{e}_j + \mathbf{e}_i \cdot \partial_\alpha \mathbf{e}_j n_j \\ &= \partial_\alpha n_i + \epsilon_{ij} A_\alpha n_j, \end{aligned} \tag{13}$$

where $\epsilon_{ij} A_\alpha = \mathbf{e}_i \cdot \partial_\alpha \mathbf{e}_j$ is called the spin-connection. The final line is justified because the derivative of any unit vector is perpendicular to this unit vector. More generally, the covariant derivative of the vector $\mathbf{n}$ along x^α is [17]

$$D_\alpha n^\beta = \partial_\alpha n^\beta + \Gamma^\beta_{\alpha\gamma} n^\gamma, \tag{14}$$

where the Christoffel symbols are

$$\Gamma^\alpha_{\beta\gamma} = \frac{1}{2} g^{\alpha\delta} \left(\partial_\gamma g_{\beta\delta} + \partial_\beta g_{\delta\gamma} - \partial_\delta g_{\beta\gamma} \right). \tag{15}$$

Finally, with the antisymmetric tensor and the area element in hand we can state a useful formula in integral calculus, namely Stokes' theorem

$$\int d^2x \sqrt{g} \gamma^{\alpha\beta} D_\alpha n_\beta = \oint dx^\alpha n_\alpha. \tag{16}$$

1.3.2 *Curvature*

The curvature is the deviation from flatness and therefore a measure of the rate of change of the tangent vectors along the normal,

or, put the other way around, a measure of the rate of change of the normal along the tangent vectors. This can be cast in a curvature tensor defined as

$$K_{\alpha\beta} = \mathbf{N} \cdot \partial_\beta \mathbf{t}_\alpha = -\mathbf{t}_\beta \cdot \partial_\alpha \mathbf{N}. \tag{17}$$

From this tensor we extract the intrinsic Gaussian curvature

$$G = \det\left(K^\alpha_\beta\right) = \frac{1}{2}\gamma^{\alpha\gamma}\gamma^{\beta\delta}K_{\alpha\beta}K_{\gamma\delta} = \kappa_1\kappa_2, \tag{18}$$

and extrinsic mean curvature

$$H = \frac{1}{2}\mathrm{Tr}\left(K^\alpha_\beta\right) = \frac{1}{2}g^{\alpha\beta}K_{\alpha\beta} = \frac{1}{2}\left(\kappa_1 + \kappa_2\right), \tag{19}$$

where $\kappa_1 = \mathbf{N} \cdot \partial_1 \tilde{\mathbf{e}}_1$ and $\kappa_2 = \mathbf{N} \cdot \partial_2 \tilde{\mathbf{e}}_2$ are the extremal or principal curvatures, the curvature in the principal directions $\tilde{\mathbf{e}}_1$ and $\tilde{\mathbf{e}}_2$. These eigenvalues and eigenvectors can be obtained by diagonalising the matrix associated with the curvature tensor. If at a point on a surface κ_1 and κ_2 have the same sign, the Gaussian curvature is positive and from the outsiders' point of view the surface curves away in the same direction whichever way you go, as is the case on mountaintops, or peaks and in valleys. In contrast, if at a point on a surface κ_1 and κ_2 have opposite signs the Gaussian curvature is negative, the saddle-like surface curves away in opposite directions. The magnitude of κ_1 and κ_2 is equal to the inverse of the radius of the tangent circle in the principal direction (Fig. 2). It turns out that the Gaussian curvature and the spin-connection are related. We will see how in a moment by considering the normal (third) component of the curl (denoted by $\nabla\times$) of the spin-connection

$$\begin{aligned}
\left(\nabla \times \mathbf{A}\right)_3 &= \epsilon_{3jk}\partial_j\left(\mathbf{e}_1 \cdot \partial_k \mathbf{e}_2\right) \\
&= \epsilon_{3jk}\partial_j \mathbf{e}_1 \cdot \partial_k \mathbf{e}_2 \\
&= \epsilon_{3jk}\left(\mathbf{N} \cdot \partial_j \mathbf{e}_1\right)\left(\mathbf{N} \cdot \partial_k \mathbf{e}_2\right),
\end{aligned} \tag{20}$$

where we have used the product rule and the antisymmetry of ϵ_{ijk} in the second equality sign. The final line is justified by the fact that the derivative of a unit vector is perpendicular to itself and therefore we have *e.g.* $\partial_j \mathbf{e}_1 = \left(\mathbf{N} \cdot \partial_j \mathbf{e}_1\right)\mathbf{N} + \left(\mathbf{e}_2 \cdot \partial_j \mathbf{e}_1\right)\mathbf{e}_2$. If we now with the aid of eqs. (17) and (18) note that

$$G = \left(\mathbf{N} \cdot \partial_1 \mathbf{e}_1\right)\left(\mathbf{N} \cdot \partial_2 \mathbf{e}_2\right) - \left(\mathbf{N} \cdot \partial_1 \mathbf{e}_2\right)\left(\mathbf{N} \cdot \partial_2 \mathbf{e}_1\right), \tag{21}$$

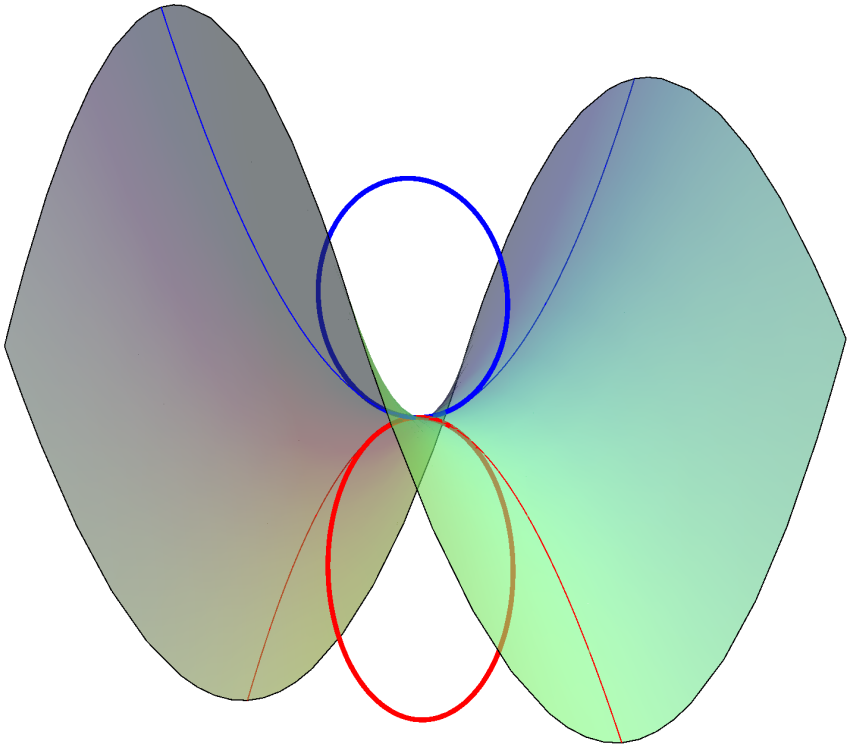

Figure 2: A saddle surface has negative Gaussian curvature, as κ_1 and κ_2 have different signs. The magnitudes of the curvatures κ_1 and κ_2 are given by the inverse radii of the tangent circles drawn in blue and red.

we easily see that the normal component of the curl of the spin-connection equals the Gaussian curvature:

$$(\nabla \times \mathbf{A}) \cdot \mathbf{N} = G, \tag{22}$$

or alternatively [73]

$$\gamma^{\alpha\beta} D_\alpha A_\beta = G. \tag{23}$$

This geometric interpretation of $\mathbf{A}$ will show its importance in section 1.4, where we will comment on its implications on the geometric frustration in curved nematic liquid crystal films.

Finally, a popular choice of parametrisation of the surface is the Monge gauge or height representation in which $\mathbf{x} = (x, y)$ and $\mathbf{R} = (x, y, f(x, y))$, where $f(x, y)$ is the height of the surface

above the xy-plane. In this representation the Gaussian curvature reads

$$G = \frac{\det \partial_\alpha \partial_\beta f}{g}, \tag{24}$$

where the determinant of the metric is given by

$$g = 1 + (\partial_x f)^2 + (\partial_y f)^2 . \tag{25}$$

1.4 ELASTICITY ON CURVED SURFACES AND IN CONFINED GEOMETRIES

1.4.1 *Elasticity of a two-dimensional nematic liquid crystal*

In a nematic liquid crystal the molecules (assumed to be anisotropic) tend to align parallel to a common axis. The direction of this axis is labeled with a unit vector, $\mathbf{n}$, called the director (see Fig. 3). The states $\mathbf{n}$ and $-\mathbf{n}$ are equivalent. Any spatial distortion of a uniform

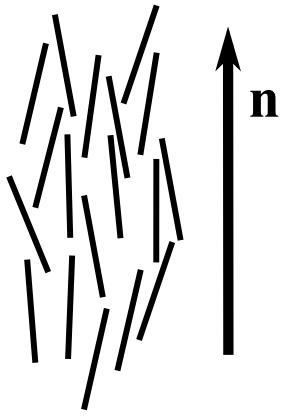

Figure 3: The director $\mathbf{n}$ specifies the average local orientation of the nematic molecules.

director field costs energy. If we assume that these deformations are small on the molecular length scale, l,

$$|\partial_i n_j| \ll \frac{1}{l}, \tag{26}$$

we can construct a phenomenological continuum theory. The resulting Frank free energy F for a two dimensional flat nematic liquid crystal reads [18, 39, 40]

$$F = \frac{1}{2} \int d^2x \left[k_1 \left(\partial_i n_i\right)^2 + k_3 \left(\epsilon_{ij} \partial_i n_j\right)^2 \right], \tag{27}$$

where the splay and bend elastic constants, k_1 and k_3 respectively, measure the energy of the two independent distortions shown in Fig. 4. To simplify the equations, one often makes the assumption

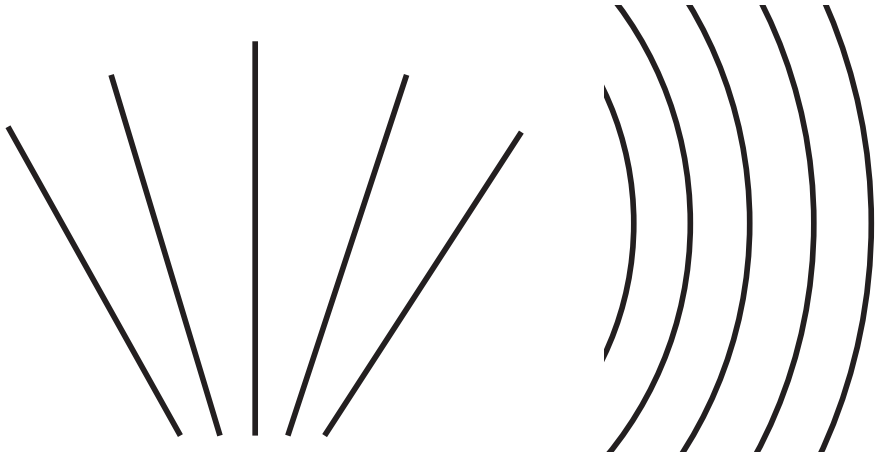

Figure 4: Conformations with (left panel) a non-vanishing divergence of the director and (right panel) a non-vanishing curl of the director.

of isotropic elasticity. In this approximation the Frank elastic constants are equal, $k_1 = k_3 = k$, and up to boundary terms the free energy reduces to [39]

$$F = \frac{1}{2}k \int d^2x \partial_i n_j \partial_i n_j. \tag{28}$$

When the coupling of the director to the curvature tensor $K_{\alpha\beta}$ [82, 38, 36, 26, 62, 84, 67, 66, 68] is ignored, the elastic free energy on a curved surface generalises to [58, 78, 70, 104, 105]

$$F = \frac{1}{2}k \int d^2x \sqrt{g} D_\alpha n^\beta D^\alpha n_\beta. \tag{29}$$

In this equation the area element has become $dS = d^2x\sqrt{g}$ and partial derivatives have been promoted to covariant derivatives. Because the director is of unit length, we can conveniently specify it in terms of its angle with a local orthonormal reference frame, $\Theta(\mathbf{x})$, as follows

$$\mathbf{n} = \cos\Theta\, \mathbf{e_1} + \sin\Theta\, \mathbf{e_2}. \tag{30}$$

Then, since $\partial_\alpha n_1 = -\sin\Theta\, \partial_\alpha\Theta = -n_2\partial_\alpha\Theta$ and similarly $\partial_\alpha n_2 = \cos\Theta\, \partial_\alpha\Theta = n_1\partial_\alpha\Theta$ we see that

$$\partial_\alpha n_i = -\epsilon_{ij} n_j \partial_\alpha\Theta, \tag{31}$$

with which we find the covariant derivative to be

$$D_\alpha n_i = -\epsilon_{ij} n_j \left(\partial_\alpha \Theta - A_\alpha\right). \tag{32}$$

Therefore, we can rewrite the elastic energy as [73]

$$F = \frac{1}{2} k \int d^2x \sqrt{g} \left(\partial_\alpha \Theta - A_\alpha\right) \left(\partial^\alpha \Theta - A^\alpha\right), \tag{33}$$

where we have used that $\left(-\epsilon_{ij} n_j\right)\left(-\epsilon_{ij} n_j\right) = \delta_{jk} n_j n_k = \cos^2(\Theta) + \sin^2(\Theta) = 1$. This form of the free energy clearly shows that nematic order on a curved surface is geometrically frustrated. The topological constraints of the introductory section are merely a special example of the frustration of local order due to the geometric properties of the system. Note that for a curved surface without such a topological constraint (*e.g.* a Gaussian bump) the ground state can be a deformed director field. Since the curl of the spin-connection equals the Gaussian curvature (eq. (23)), if the Gaussian curvature is nonzero, the spin-connection is irrotational and cannot be written as the gradient of a scalar field, $A_\alpha \neq \partial_\alpha \Theta$, just like the magnetic field cannot be described by a scalar field either. Therefore, F in eq. (33) is nonzero and we can conclude that there is geometric frustration present in the system.

1.4.2 *Elasticity of a two-dimensional solid*

Similar to the construction of the continuum elastic energy of a nematic liquid crystal, we can write down the elastic energy of a linear elastic solid as an integral of terms quadratic in the deformations, *i.e.* strain. This strain is found in the following way. Consider a point $\mathbf{x} = (x, y, 0)$ on an initially flat solid. This point is displaced to $\mathbf{x}'(\mathbf{x}) = (x', y', f)$ in the deformed solid, and so we may define a displacement vector $\mathbf{u}(\mathbf{x}) = \mathbf{x}' - \mathbf{x} = u_x \mathbf{e}_x + u_y \mathbf{e}_y + f \mathbf{e}_z$. The square of the line element in the deformed plate is then given by $ds'^2 = (dx + du_x)^2 + (dx + du_x)^2 + df^2$. Noting that $du_x = \partial_i u_x dx_i$ with $x_i = x, y$ and similarly for u_y and f we find [44]

$$ds'^2 = ds^2 + 2u_{ij} dx_i dx_j. \tag{34}$$

Thus, the strain tensor $u_{ij}(\mathbf{x})$ encodes how infinitesimal distances change in the deformed body with respect to the resting state of the solid and reads

$$u_{ij} = \frac{1}{2}\left(\partial_i u_j + \partial_j u_i + A_{ij}\right), \tag{35}$$

where we have omitted non-linear terms of second order in $\partial_i u_j$ and where the tensor field $A_{ij}(\mathbf{x})$ is now defined as

$$A_{ij} \equiv \partial_i f \partial_j f. \tag{36}$$

We will assume that curvature plays its part only through this coupling of gradients of the displacement field to the geometry of the surface, and we will therefore adopt the flat space metric. This is a valid approximation for moderately curved solids, as we comment on at the end of the section [107, 6]. To leading order in gradients of the height function, A_{ij} is related to the curvature by (see eq. (24))

$$-\frac{1}{2}\epsilon_{ik}\epsilon_{jl}\partial_k\partial_l A_{ij} = \det(\partial_i\partial_j f) = G. \tag{37}$$

Isotropy of the solid leaves two independent scalar combinations of u_{ij} that contribute to the stretching energy [44]:

$$F = \frac{1}{2}\int dS \left(2\mu u_{ij}^2 + \lambda u_{ii}^2\right). \tag{38}$$

The elastic constants λ and μ are called the Lamé coefficients. Minimisation of this energy with respect to u_j leads to the force balance equation:

$$\partial_i \sigma_{ij} = 0, \tag{39}$$

where the stress tensor $\sigma_{ij}(\mathbf{x})$ is defined by Hooke's law

$$\sigma_{ij} = 2\mu u_{ij} + \lambda \delta_{ij} u_{kk}. \tag{40}$$

The force balance equation can be solved by introducing the Airy stress function, $\chi(\mathbf{x})$, which satisfies

$$\sigma_{ij} = \epsilon_{ik}\epsilon_{jl}\partial_k\partial_l\chi, \tag{41}$$

since this automatically gives

$$\partial_i\sigma_{ij} = \epsilon_{jk}\partial_k\left[\partial_1, \partial_2\right]\chi = 0 \tag{42}$$

by the commutation of the partial derivatives. If one does not adopt the flat space metric, the covariant generalisation of the force balance equation is not satisfied, because the the commutator of the covariant derivatives, known as the Riemann curvature tensor, does not vanish. It is actually proportional to the Gaussian curvature and indicates why the range of validity of this approach is limited to moderately curved surfaces [107, 6]. Finally, for small $\partial_i u_j$ the bond angle field, $\Theta(\mathbf{x})$, is given by

$$\Theta = \frac{1}{2}\epsilon_{ij}\partial_i u_j. \tag{43}$$

1.4.3 *Elasticity of a three-dimensional nematic liquid crystal*

Besides splay and bend, there are two other deformations possible in a three-dimensional nematic liquid crystal. They are twist and saddle-splay, measured by elastic moduli K_2 and K_{24}. Twist refers to a helical type of deformation for which the rotation of $\mathbf{n}$ has a component along $\mathbf{n}$. The analog of eq. (27) reads

$$\begin{aligned} F[\mathbf{n}(\mathbf{x})] = \frac{1}{2}\int dV \Big(& K_1 (\nabla \cdot \mathbf{n})^2 \\ & + K_2 (\mathbf{n} \cdot \nabla \times \mathbf{n})^2 + K_3 (\mathbf{n} \times \nabla \times \mathbf{n})^2 \Big) \\ & - K_{24} \int \mathbf{dS} \cdot (\mathbf{n} \nabla \cdot \mathbf{n} + \mathbf{n} \times \nabla \times \mathbf{n}) . \end{aligned} \tag{44}$$

The integration of the splay, twist and bend energy density is over the volume to which the nematic is confined. The saddle-splay energy per unit volume is a pure divergence term, hence the saddle-splay energy can be written as the surface integral in eq. (44). In addition to the energy in eq. (44), there is an energetic contribution coming from the interfacial interactions, often larger in magnitude. Therefore, the anchoring of the nematic molecules at the boundary can be taken as a constraint. In one of the possible anchoring conditions the director is forced to be tangential to the surface, yet free to rotate in the plane. In this case of planar degenerate boundary conditions, we derive in chapter 4 that the saddle-splay energy reduces to

$$F_{24} = K_{24} \int dS \left(\kappa_1 n_1^2 + \kappa_2 n_2^2 \right), \tag{45}$$

thus coupling the director to the curvature of the boundary surface.

1.5 TOPOLOGICAL DEFECTS

Topological defects are characterised by a small region where the order is not defined. Topological defects in translationally ordered media, such as crystals, are called *dislocations*. Defects in the orientational order, such as in nematic liquid crystals and again crystals, are called *disclinations*. The defects are topological when they cannot be removed by a continuous deformation of the order parameter. As we will see momentarily, they are classified according to a topological quantum number or topological charge, a quantity

that may only take on a discrete set of values and which can be measured on any circuit surrounding the defect.

1.5.1 *Disclinations in a nematic*

Consider for concreteness a two-dimensional nematic liquid crystal. A singularity in the director field is an example of a disclination. Such a point defect can be classified by its winding number, strength, or topological charge, s, which is the number of times the director rotates by 2π, when following one closed loop in counterclockwise direction around the singularity:

$$\oint d\Theta = \oint dx^\alpha \partial_\alpha \Theta = 2\pi s. \tag{46}$$

We can express eq. (46) in differential form by invoking Stokes' theorem:

$$\gamma^{\alpha\beta} D_\alpha \partial_\beta \Theta = q\delta\left(\mathbf{x} - \mathbf{x}_a\right), \tag{47}$$

where we use an alternative labelling, $q = 2\pi s$, of the charge of the defect, which is located at $\mathbf{x}_a$. The delta-function obeys

$$\delta\left(\mathbf{x} - \mathbf{x}_a\right) = \frac{\delta\left(x^1 - x_a^1\right)\delta\left(x^2 - x_a^2\right)}{\sqrt{g}}, \tag{48}$$

such that the integral over the surface yields one. The far-field contribution of the defect to the angular director in a flat plane reads

$$\Theta = s\phi + c, \tag{49}$$

as it forms a solution to the Euler-Lagrange equation of the elastic free energy:

$$\partial^2 \Theta = 0. \tag{50}$$

Here, ϕ is the azimuthal angle and c is just a phase. Examples are presented in Fig. 5. Note that since the states $\mathbf{n}$ and $-\mathbf{n}$ are equivalent, defects with half-integer strength are also possible. In fact, it is energetically favourable for an $s = 1$ defect to unbind into two $s = \frac{1}{2}$ defects [70, 75].

These defects can be detected experimentally by crossed-polarised microscopy. The image will appear black there where the director

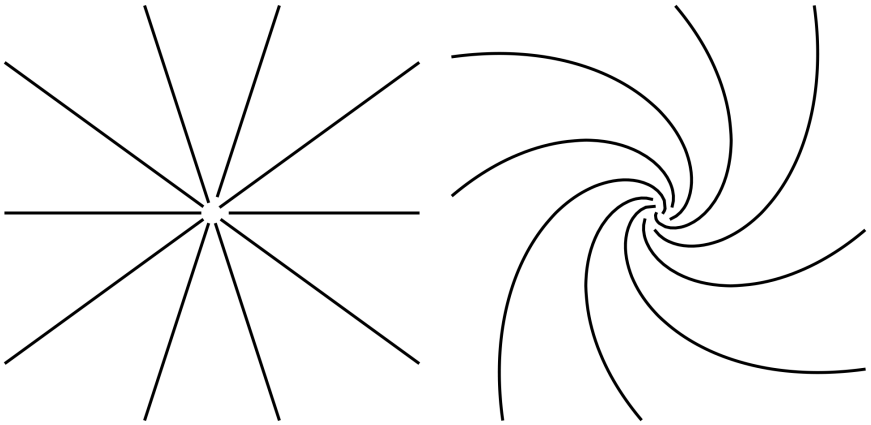

(a) $s = 1$, $c = 0$

(b) $s = 1$, $c = \frac{\pi}{4}$

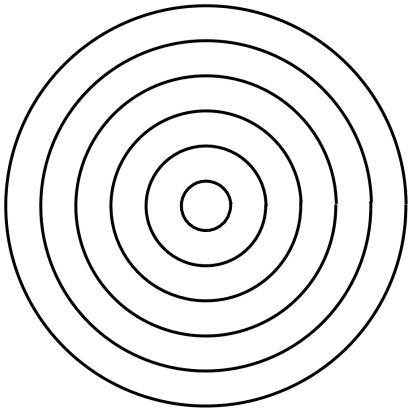

(c) $s = 1$, $c = \frac{\pi}{2}$

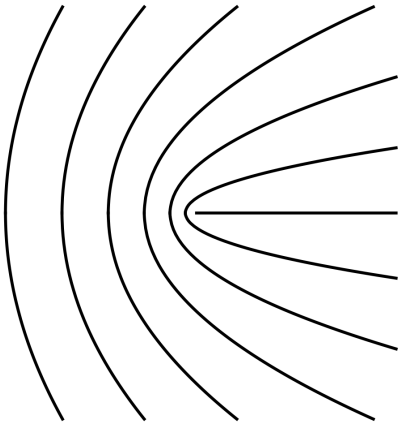

(d) $s = \frac{1}{2}$, $c = 0$

Figure 5: Director configurations, $n_1 = \cos\Phi$, $n_2 = \sin\Phi$, for disclinations of strength s and constant c.

is aligned with one of the polarisers (and thus perpendicular to the other polariser). Therefore, there are two black (and two coloured) brushes meeting at an $s = \pm 1/2$ defect. There are four black (and four coloured) brushes meeting at an $s = \pm 1$ defect.

1.5.2 *Disclinations in a crystal*

Though energetically more costly, disclinations also arise in two-dimensional crystals. At these points, the coordination number deviates from its ordinary value, which is six for a crystal on a triangular lattice. Just like in nematic liquid crystals, disclinations in crystals are labelled by a topological charge, q, which is the angle

over which the vectors specifying the lattice directions rotate when following a counterclockwise circuit around the disclination. If we parametrise these lattice direction vectors with $\Theta(\mathbf{x})$, the bond-angle field, this condition reads mathematically

$$\oint d\Theta = q. \tag{51}$$

Thus for disclinations in a triangular lattice with five-fold and seven-fold symmetry, as displayed in Fig. 6, $q = \frac{\pi}{3}$ and $q = -\frac{\pi}{3}$ respectively. Analogous to eq. (47), the flat-space differential form

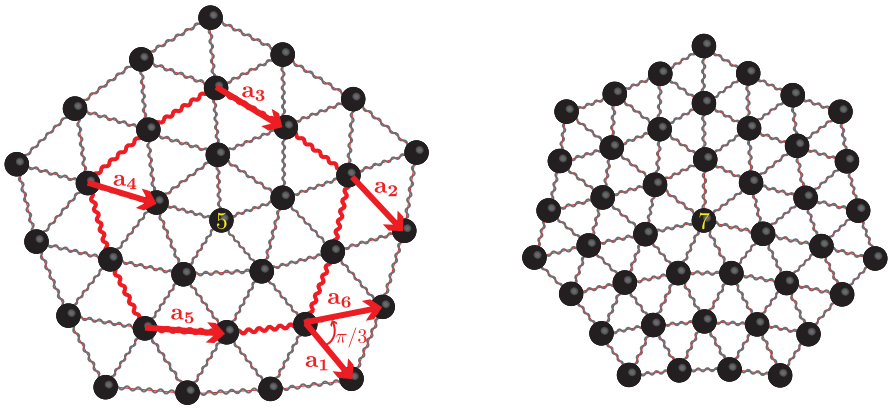

Figure 6: (Left panel) Five-fold and (right panel) seven-fold disclination. When following a closed counterclockwise loop (red) around the five-fold disclination, the initial lattice vector $\mathbf{a}_1$ rotates via $\mathbf{a}_2$, $\mathbf{a}_3$, $\mathbf{a}_4$ and $\mathbf{a}_5$ over an angle of $\pi/3$ to $\mathbf{a}_6$.

of eq. (51) for a disclination located at $\mathbf{x}_a$ reads

$$\epsilon_{ij}\partial_i\partial_j\Theta = q\delta(\mathbf{x} - \mathbf{x}_a). \tag{52}$$

1.5.3 *Dislocations*

Besides disclinations, dislocations can occur in crystals. Dislocations are characterised by a Burgers vector $\mathbf{b}$. This vector measures the change in the displacement vector, if we make a counterclockwise loop surrounding the dislocation,

$$\oint d\mathbf{u} = \mathbf{b}. \tag{53}$$

Just as the strength of disclinations can only take values from a discrete set, the Burgers vector of a dislocation is equal to some integer multiple of a lattice vector. Also note that a dislocation

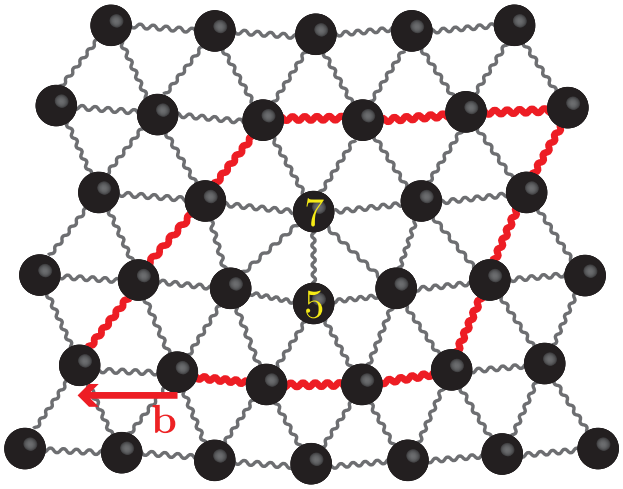

Figure 7: Dislocation in a triangular lattice. The Burgers vector specifies by how much a clockwise circuit (marked in red, bold) around the dislocation fails to close. A dislocation can be viewed as disclination dipole with a moment perpendicular to its Burgers vector.

can be viewed as a pair of closely spaced disclinations of opposite charge [71], as can be seen in Fig. 7.

The flat-space differential form of eq. (53) for a dislocation at $\mathbf{x}_a$ is

$$\epsilon_{ij}\partial_i\partial_j u_k = b_k \delta\left(\mathbf{x} - \mathbf{x}_a\right), \tag{54}$$

which again can be obtained by using Stokes' theorem.

1.6 INTERACTION BETWEEN CURVATURE AND DEFECTS

1.6.1 *Coupling in liquid crystals*

It is possible to recast the free energy in terms of the locations of the topological defects rather than the director or displacement field, if smooth (*i.e.* non-singular) deformations are ignored. In this case the energy in eq. (33) is minimised with respect to Θ, which leads to

$$D^\alpha\left(\partial_\alpha\Theta - A_\alpha\right) = 0. \tag{55}$$

This needs to supplemented with an equation for the effective charge distribution:

$$\gamma^{\alpha\beta} D_\alpha\left(\partial_\beta\Theta - A_\beta\right) = \rho - G, \tag{56}$$

obtained by combining eq. (23) for the curvature and eq. (47) for the defect density $\rho(\mathbf{x})$,

$$\rho = \sum_a q_a \delta(\mathbf{x} - \mathbf{x}_a). \tag{57}$$

Eq. (55) is automatically satisfied if one chooses [104]

$$\partial_\alpha \Theta - A_\alpha = \gamma_\alpha{}^\beta \partial_\beta \chi, \tag{58}$$

where $\chi(\mathbf{x})$ is an auxiliary function. At the same time, substituting eq. (58) into eq. (56) leads to

$$-D^2\chi = \rho - G. \tag{59}$$

The source in this Poisson equation contains both topological point charges as well as the Gaussian curvature with opposite sign. The analog of the electrostatic potential is χ. The role of the electric field is played by $\partial_\alpha \chi$. Indeed, substituting eq. (58) in eq. (33), shows that the energy density is proportional to the square of the electric field:

$$F = \frac{1}{2} k \int dS \partial_\alpha \chi \partial^\alpha \chi. \tag{60}$$

Next, we formally solve eq. (59)

$$\chi = -\int dS' \Gamma_L\left(\mathbf{x}, \mathbf{x}'\right)\left(\rho\left(\mathbf{x}'\right) - G\left(\mathbf{x}'\right)\right), \tag{61}$$

where $\Gamma_L(\mathbf{x}, \mathbf{x}')$ is the Green function of the Laplace-Beltrami operator, $D^2 = D_\alpha D^\alpha$, satisfying

$$D^2 \Gamma_L\left(\mathbf{x}, \mathbf{x}'\right) = \delta\left(\mathbf{x} - \mathbf{x}'\right). \tag{62}$$

Integrating eq.(60) by parts and substituting our expressions for χ and the Laplacian of χ (eqs. (61) and (59) respectively) results (up to boundary terms) in

$$F = -\frac{k}{2} \int dS \int dS' \left(\rho(\mathbf{x}) - G(\mathbf{x})\right) \Gamma_L\left(\mathbf{x}, \mathbf{x}'\right)\left(\rho\left(\mathbf{x}'\right) - G\left(\mathbf{x}'\right)\right), \tag{63}$$

from which we again deduce the analogy with two-dimensional electrostatics. In this analogy the defects are electric point sources with their electric charge equal to the topological charge q and the Gaussian curvature with its sign reversed is a background charge

distribution. Therefore the defects will be attracted towards regions of Gaussian curvature with the same sign as the topological charge [58, 7, 104, 106, 113, 35, 84, 100]. Such screening will be perfect if $S = \rho$ everywhere, since $F = 0$ then. However, unless the surface contains singularities in the Gaussian curvature, like the apex of a cone, perfect screening will be impossible, as the topological charge is quantised whereas the Gaussian curvature is typically smoothly distributed.

1.6.2 *Coupling in crystals*

Note that an *arbitrary* field χ solves eq. (42). However, χ must be physically possible and we therefore need to accompany eq. (42) with another equation, which we will obtain by considering the inversion of eq. (40) [44, 85]:

$$u_{ij} = \frac{1+\nu}{Y}\sigma_{ij} - \frac{\nu}{Y}\sigma_{kk}\delta_{ij} \tag{64}$$

$$= \frac{1+\nu}{Y}\epsilon_{ik}\epsilon_{jl}\partial_k\partial_l\chi - \frac{\nu}{Y}\partial^2\chi\delta_{ij} \tag{65}$$

where the two-dimensional Young's modulus, Y, and Poisson ratio, ν, are given by

$$Y = \frac{4\mu\left(\mu+\lambda\right)}{2\mu+\lambda}, \tag{66}$$

$$\nu = \frac{\lambda}{2\mu+\lambda}. \tag{67}$$

Applying $\epsilon_{ik}\epsilon_{jl}\partial_k\partial_l$ to eq. (65) gives

$$\frac{1}{Y}\partial^4\chi = \epsilon_{ik}\epsilon_{jl}\partial_k\partial_l u_{ij}. \tag{68}$$

By invoking eqs. (35), (43), the differential expressions for the defects, namely eqs. (54) and (52), as well as eq. (37) for the curvature, one can rewrite the right hand side to arrive at the crystalline analog of eq. (59):

$$\frac{1}{Y}\partial^4\chi = \rho - G, \tag{69}$$

where the defect distribution, ρ, of disclinations with charge q_a and dislocations with Burgers vector $\mathbf{b}^b$ reads

$$\rho = \sum_a q_a\delta\left(\mathbf{x}-\mathbf{x}_a\right) + \sum_b \epsilon_{ij}b_i^b\partial_j\delta\left(\mathbf{x}-\mathbf{x}_b\right). \tag{70}$$

We can also rewrite the free energy (up to boundary terms) in terms of the Airy stress function as follows:

$$F = \frac{1}{2Y} \int dS \left(\partial^2 \chi\right)^2 . \tag{71}$$

If we integrate this by parts twice and use eq. (69) to eliminate χ and $\partial^4 \chi$, we find (up to boundary terms)

$$F = \frac{Y}{2} \int dS \int dS' \left(\rho\left(\mathbf{x}\right) - G\left(\mathbf{x}\right)\right) \Gamma_B \left(\mathbf{x}, \mathbf{x}'\right) \left(\rho\left(\mathbf{x}'\right) - G\left(\mathbf{x}'\right)\right) \tag{72}$$

where Γ_B is the Greens function of the biharmonic operator

$$\partial^4 \Gamma_B \left(\mathbf{x}, \mathbf{x}'\right) = \delta\left(\mathbf{x} - \mathbf{x}'\right). \tag{73}$$

Eq. (72) is the crystalline analog of eq. (63). Again, the defects can screen the Gaussian curvature. The interaction, however, is different than the Coulomb interaction in the liquid crystalline case. If the surface is allowed to bend, disclinations will induce buckling, illustrated in Fig. 8 with paper models. In these cones, the integrated Gaussian curvature is determined by the angular deficit of the disclination

$$\int dSG = q. \tag{74}$$

If there are no topological defects (implying that $\rho = 0$ in eq. (69)), but the curvature still provides a source of stress of the Airy stress function χ^G:

$$\frac{1}{Y} \partial^4 \chi^G = -G. \tag{75}$$

One can solve this equation in two steps. First, we make use of an auxiliary function U obeying

$$\partial^2 U = G. \tag{76}$$

This leaves the following equation to be solved (*i.e.* the second step)

$$\frac{1}{Y} \partial^2 \chi^G = -U + U_H, \tag{77}$$

where U_H is a harmonic function (*i.e.* satisfying $\partial^2 U_H = 0$) introduced to fulfil the boundary conditions [107].

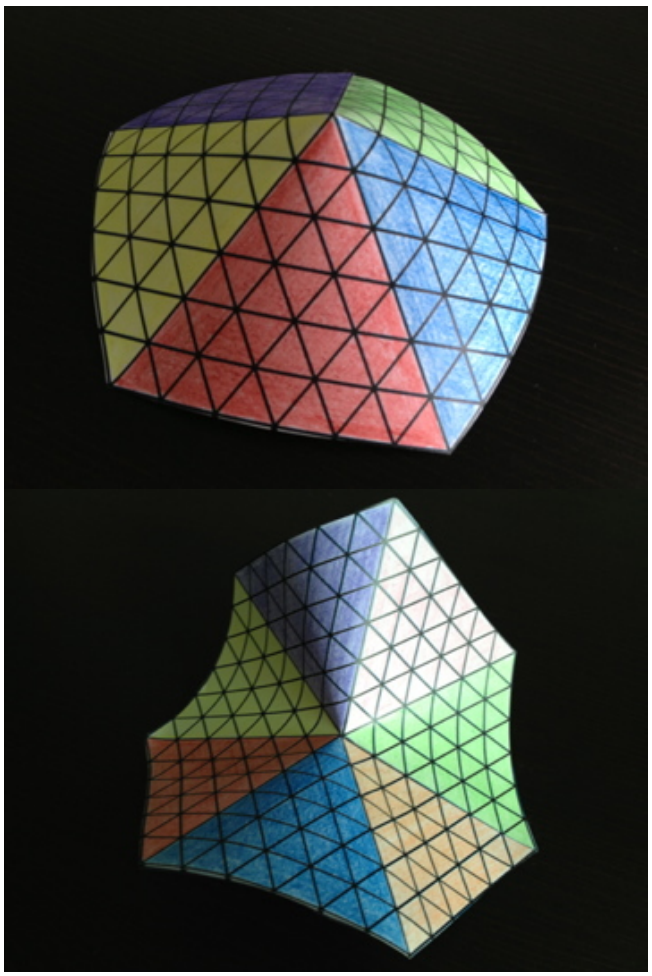

Figure 8: Paper models illustrating the coupling between disclinations and curvature. *Top panel:* 5-fold (*Bottom panel*: 7-fold) coordinated particle in a triangular lattice. Positively (negatively) charged disclinations and positive (negative) Gaussian curvature attract.

Surprisingly, charge-neutral dislocations and pleats can also screen the curvature [73, 85, 107, 32, 34]. Pleats are formed by arrays of dislocations and allow for an extra piece of crystal, just like their fabric analogs. Since the opening angle of pleats, approximately equal to $n_d a$ with a the lattice spacing and n_d the dislocation line density can be arbitrarily small, pleats can actually provide a finer screening than quantised disclinations.

1.7 NEMATIC ORDER ON THE SPHERE

As a naive guess for the ground state of a two-dimensional nematic liquid crystal phase on the surface of the sphere, one could imagine the excess of topological charge to be located at the poles, like in the case of tilted molecules on the sphere. However, the order parameter, the director, has the symmetry of a headless arrow instead of a vector. Therefore, this makes it possible for the two $s = 1$ defects to unbind into four $s = \frac{1}{2}$ defects relaxing at the vertices of a regular tetrahedron [57]. The baseball-like nematic texture is illustrated in Fig. 9. The repulsive nature of defects with

Figure 9: The baseball-like ground state of a two-dimensional spherical nematic coating has four $s = \frac{1}{2}$ at the vertices of a tetrahedron in the one-constant approximation. Reprinted figure with permission from ref. [105]. Copyright 2006 by the American Physical Society.

like charges can be seen from the free energy, which, as shown in the previous section, can be reformulated entirely in terms of the defects rather than the director [70, 57]:

$$F = -\frac{\pi k}{2} \sum_{i \neq j} s_i s_j \log\left(1 - \cos\theta_{ij}\right) + E\left(R\right) \sum_j s_j^2. \tag{78}$$

Here, θ_{ij} is the angular separation between defects i and j, *i.e.* $\theta_{ij} = \frac{d_{ij}}{R}$, with d_{ij} being the geodesic distance. The first term yields the long-range interaction of the charges. The second term accounts for the defect self-energy

$$E(R) = \pi k \log\left(\frac{R}{b}\right) + E_c, \tag{79}$$

where we have imposed a cut-off b representing the defect core size, which has energy E_c. This cut-off needs to be introduced in order to prevent the free energy from diverging. Heuristically, this logarithmically diverging term in the free energy is responsible for the splitting of the two $s = 1$ defects into four $s = \frac{1}{2}$ defects. Two $s = 1$ defects contribute $\left(2 \times 1^2\right) \pi k \log\left(\frac{R}{b}\right) = 2\pi k \log\left(\frac{R}{b}\right)$ to the free energy, whereas four $s = \frac{1}{2}$ defects contribute only $\left(4 \times \left(\frac{1}{2}\right)^2\right) \pi k \log\left(\frac{R}{b}\right) = \pi k \log\left(\frac{R}{b}\right)$.

In addition to this ground state, other defect structures have been observed in computer simulations [23, 90, 88, 3]. If there is a strong anisotropy in the elastic moduli, the four defects are found to lie on a great circle rather than the vertices of a regular tetrahedron [88, 3].

1.8 THIS THESIS

1.8.1 *Spherical nematic shells (part I)*

An experimental model system of spherical nematics is a nematic double emulsion droplet [24, 54, 56, 49, 55, 86, 50, 41, 51]. This is a structure in which a water droplet is captured by a larger nematic liquid crystal droplet, which in turn is dispersed in an outer fluid (Fig. 10). There are some crucial differences between a two-dimensional spherical nematic and a nematic double emulsion droplet. Not only is the nematic coating of a finite thickness, this thickness can be inhomogeneous as a result of buoyancy-driven displacement (or other mechanisms) of the inner droplet out of the centre of the nematic droplet.

Like point disclinations in two dimensions, there exist disclination *lines* in a three-dimensional nematic liquid crystal, which are categorised in similar fashion. However, charge-one lines, and integral lines in general, do not exist. Such lines lose their singular cores [12, 63] by 'escaping in the third dimension'. In shells, such

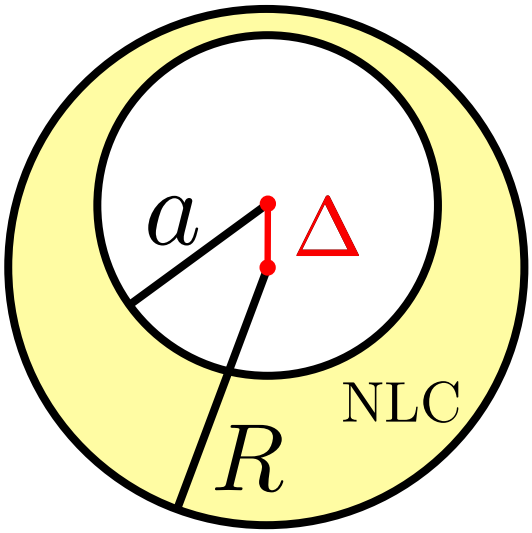

Figure 10: Schematic of a nematic double emulsion droplet of radius R. The inner water droplet of radius a is displaced by an amount Δ along the vertical direction, thereby making the top of the shell thinner.

an escape leads to another type of defect, namely point defects at the interface, known as boojums (Fig. 11).

In a spherical nematic layer of *finite* thickness, the baseball structure with four $s = \frac{1}{2}$ disclination lines spanning the shell, becomes energetically less favourable than two antipodal pairs of boojums beyond a critical thickness [105]. Instead of unbinding, the singular lines escape in the third dimension, leaving two pairs of boojums on the bounding surfaces. This divalent configuration is separated from the tetravalent configuration by a large energy barrier. As a consequence, both configurations are observed in droplets in the same emulsion. Also, trivalent shells with two $s = \frac{1}{2}$ disclination lines and one pair of boojums coexist. In chapter 2 (based on ref. [56]) we study the energetics of thin trivalent shells and find the optimal isosceles arrangement of the defects.

If, in addition, the shell thickness is inhomogeneous, the energy landscape becomes even more complex. As a consequence of the inhomogeneity the defects cluster in the thinnest part of the shell, where the length of the disclination lines (or distance between boojums forming a pair) are shorter. Since the self-energy of the disclination is proportional to its length, it is attracted towards this region of the shell. In chapter 3 (based on refs. [56, 41]), an investigation of thick and inhomogeneous divalent shells shows that

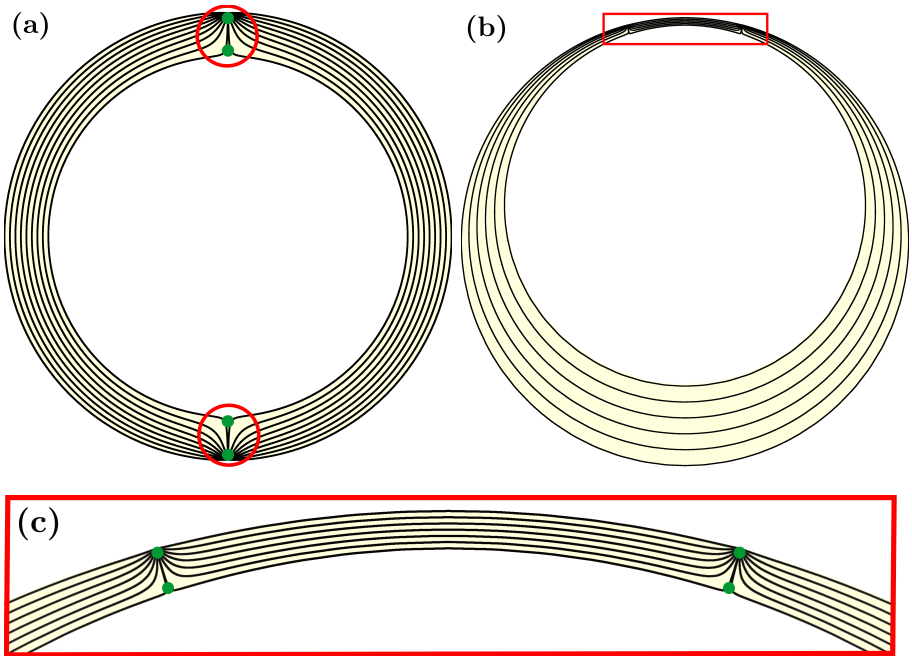

Figure 11: (a) Schematic of the deconfined defect configuration in a homogeneous shell. Two pairs (each encircled in red) of boojums, indicated by green dots, are located at the top and bottom of the shell. (b) Schematic of the confined defect configuration in an inhomogeneous shell. All boojums are located at the thinnest, top part of the shell, inside the red rectangle. (c) Zoom of the thinnest section of the inhomogeneous shell in (b).

pairs of surface defects can make abrupt transitions between the state in which the defects are confined in the thinnest part of the shell, and the deconfined state, in which the interdefect repulsion places them diametrically. These confinement and deconfinement transitions occur when the thickness or thickness inhomogeneity is varied.

1.8.2 *Toroidal nematics (part II)*

The torus has an Euler characteristic equal to zero. Hence, in a nematic droplet of toroidal shape no defects need to be present. The director field to be expected naively in such a geometry is one which follows the tubular axis, as shown in Fig. 12. This achiral director configuration contains only bend energy. In chapter 4 we show, however, that if the toroid becomes too fat it is favourable

to reduce bend deformations by twisting. The price of twisting is screened by saddle-splay deformations provided that $K_{24} > 0$ [77, 42]. The twisted configuration is chiral. Chirality stems from the Greek word for hand, and is indeed in this context easily explained: your right hand cannot be turned into a left hand by moving and rotating it. It is only when viewed in the mirror that your right hand appears to be a left hand and vica versa. Indeed, for small aspect ratios and small values of $(K_2 - K_{24})/K_3$ nematic toroids display either a right- or left-handedness despite the achiral nature of nematics. This phenomenon is recognised as spontaneous chiral symmetry breaking. Typical corresponding plots of the energy as a function of the amount of twist are shown in Fig. 12.

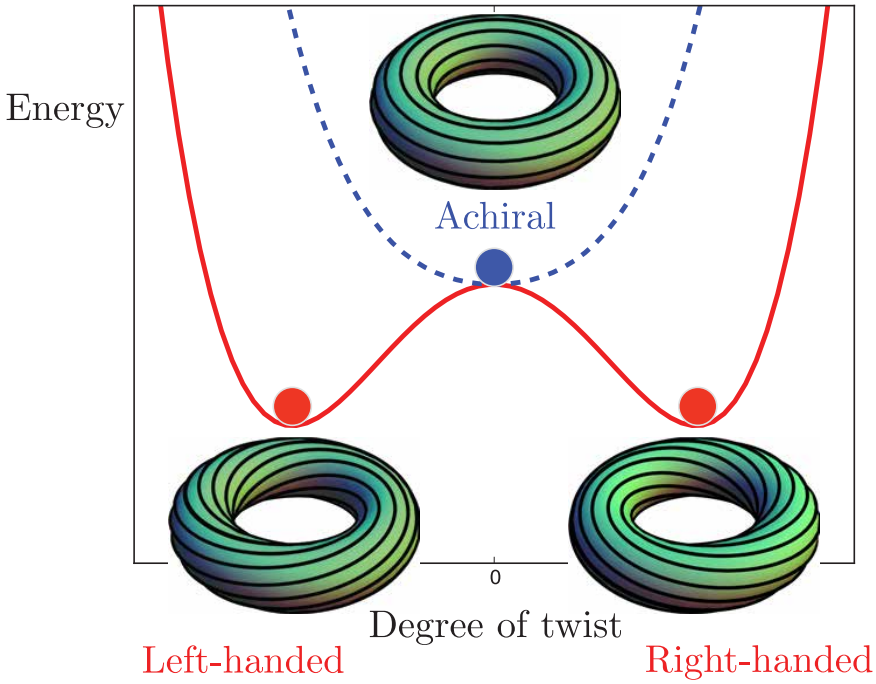

Figure 12: Energy as a function of the degree of twist has either a single achiral minimum (dashed blue) or shows spontaneous chiral symmetry breaking in toroidal nematics (red) depending on the aspect ratio and elastic constants. The chiral state is favoured for fat toroids and small values of $(K_2 - K_{24})/K_3$.

1.8.3 *Cracks in curved solids (part III)*

In chapter 5 we study cracks in curved solids rather than the crystallographic defects discussed in section 1.6.2. We consider an elastic film that is deformed into the shape of a Gaussian bump. The stresses resulting from this geometric frustration affect the onset of crack growth leading to fracture of the body. We find that the critical crack length at which growth begins depends on the location and orientation of the crack. The critical crack size can be decreased by the curvature, but also increased. In chapter 6 we calculate the path that a crack takes for several locations of the initial crack and several aspect ratios of the bump. We find that an incoming crack is deflected from the bump.